Optimization Strategies for Laser Welding High Alloy Steel Sheets

Article *in* Physics procedia · September 2014

DOI: 10.1016/j.phpro.2014.08.040

5 authors, including:

Falk Nagel
Technische Universität Ilmenau
9 PUBLICATIONS **7** CITATIONS
SEE PROFILE

Flaviu Simon
Dynardo GmbH
8 PUBLICATIONS **7** CITATIONS
SEE PROFILE

Jean Pierre Bergmann
Technische Universität Ilmenau
97 PUBLICATIONS **248** CITATIONS
SEE PROFILE

Jörg Hildebrand
Technische Universität Ilmenau
150 PUBLICATIONS **129** CITATIONS
SEE PROFILE

Available online at www.sciencedirect.com

ScienceDirect

Physics Procedia 56 (2014) 1242 – 1251

Physics Procedia

8th International Conference on Photonic Technologies LANE 2014

Optimization strategies for laser welding high alloy steel sheets

Falk Nagel[a,*], Flaviu Simon[b], Benjamin Kümmel[a], Jean Pierre Bergmann[a], Jörg Hildebrand[b]

[a]Technische Universität Ilmenau, Department of Production Technology, Neuhaus 1, 98693 Ilmenau, Germany
[b]Bauhaus-Universität Weimar, Junior Chair of Simulations and Experiments, Marienstraße 7A, 99421 Weimar, Germany

Abstract

A known phenomenon during laser welding of thin sheets is the deformation caused by thermally induced stresses. This deformation can result in a change of the gap width between the welded parts, which leads to an unstable welding process. Inducing displacements by using a second heat source will compensate for the change in gap width, hence optimizing the welding process. The base material is 1 mm thick austenitic stainless steel 1.4301, which is welded by a CO_2 laser. The second heat source is a diode laser. The gap between the welded parts was set between 0.05 mm and 0.1 mm. The influence of the second heat source on the welding process and the welding result is described. The usage of a second heat source allows a higher gap width to be set prior to the welding process. The results of the numerical simulation were found to be corresponding to those of the experiments.

Peer-review under responsibility of the Bayerisches Laserzentrum GmbH
Keywords: Laser Welding; CO_2; Diode; Distortion; Finite Element Analysis; Thermal Analysis; Mechanical Analysis; Numerical Model

1. Introduction

Laser welding is the preferred joining technology for stainless steels due to its high power density and reduced heat affected zone (HAZ). The high thermal expansion as well as the low thermal conductivity of austenitic steels is a trigger for unwanted deformations, which occur during laser welding. These deformations can either increase the gap between the welded sheets, cause them to be drawn closer together or to misalign and subsequently overlap. These problems are currently dealt with in the industry by using heavy jigs, fixings, clamps and other technologies, which restrict the relative movement of welded parts in different directions as well as increase the formation of residual stresses. While these mechanical adjustments might prove effective, they require extra financial resources and can restrict the flexibility of changes regarding the product geometry. Tack welds are state of the art in order to obtain constant weld gaps. The distance between the tack welds is supposed to range from 20 mm to 40 mm for sheets of 1 mm thickness according to Edelstahl Rostfrei (2007). However, even this method requires a lot of preparation and additional investment. This article is a proceeding for another way of countering the deformations due to laser welding of thin austenitic steel sheets. The concentrated laser heat source determines the formation of compressive and tensile

* Corresponding author. Tel.: +49-3677-69-2980 ; fax: +49-3677-69-1660 .
E-mail address: info.fertigungstechnik@tu-ilmenau.de

Peer-review under responsibility of the Bayerisches Laserzentrum GmbH
doi:10.1016/j.phpro.2014.08.040

stresses in the weld seam and in the HAZ. Residual stress is believed to be primarily caused by the compressive yielding that occurs around the molten zone when the material is heated, then expands and by the occurring tensile stress during cooling and solidification, when the metal contracts. The reduction of residual stress if further detailed in Zhao et al. (2008). These stresses and the ones from the manufacturing process cause a deformation of the parts being welded, hindering the welding process and affecting the overall quality of the final product as found in Simon et al. (2013). The objective of the investigation is to create temperature-induced displacements, which would counter the displacements from the weld process and in turn maintain a constant gap width. This can be accomplished by a secondary heat source placed at a specific location on the sheets, ahead or behind the main laser source. Due to the second heat source and the thermal expansion, the opening movement can be counteracted. A similar procedure, with the aim of countering hot cracking for an aluminium alloy has been discussed in Petzet et al. (2005).

Nomenclature

$\alpha(T)$	Temperature dependent thermal expansion coefficient	l	Element size along the weld path
ϵ	Strain	n_1	Refinement level
f^{vM}	Plastic potential	n_2	Number of time steps per element
ϵ_e	Elastic strain	P_l	Laser Power
ϵ_i	Initial strain	η_e	Power efficiency
ϵ_p	Plastic strain	Q_r	Surface flux
ϵ_{th}	Thermal strain	Q_0	Maximum flux
σ	Stress	q	Prescribed heat flux
σ_{eq}	von Mises equivalent stress	r	Radial distance
σ_y	Initial yield stress	C	Distribution width coefficient
ρ	Density	r_e	Surface radius
c_p	Specific heat	r_i	Constant input cylinder
D	Stress-Strain-Matrix	T_0	Initial temperature
h	Heat transfer coefficient	ε	Emissivity
K	Degree of stain hardening	v_w	Welding speed
T	Temperature	r_f	Focus radius
k	Thermal conductivity	t	Time
$d\lambda$	Hardening parameter	x	Current x coordinate
q_v	Volumetric heat source term	y	Current y coordinate
		z	Current z coordinate

2. Experimental and numerical procedure

2.1. Material

The stainless austenitic steel X5CrNi18-10, also known as 1.4301, was used. The chemical composition according to the supplier, is shown in Table 1. As mentioned before, this material has a relatively high coefficient of thermal

Table 1: Chemical composition of the used material.

	Fe	C	Si	Mn	Ni	P	S	Cr	N
[wt-%]	Balance	0.018	0.38	1.75	10.62	0.028	0.027	16.66	0.015

expansion and a low thermal conductivity, as seen in Fig. 1, (a) and (b). These figures describe the thermal and mechanical properties given in the Simufact.material database. The density of the material has a constant value of $7.966 \times 10^{-3}\,\mathrm{g\,mm^{-3}}$. Welding samples were cut out of the sheets using a laser. The dimensions of the samples are $300\,\mathrm{mm} \times 50\,\mathrm{mm} \times 1\,\mathrm{mm}$.

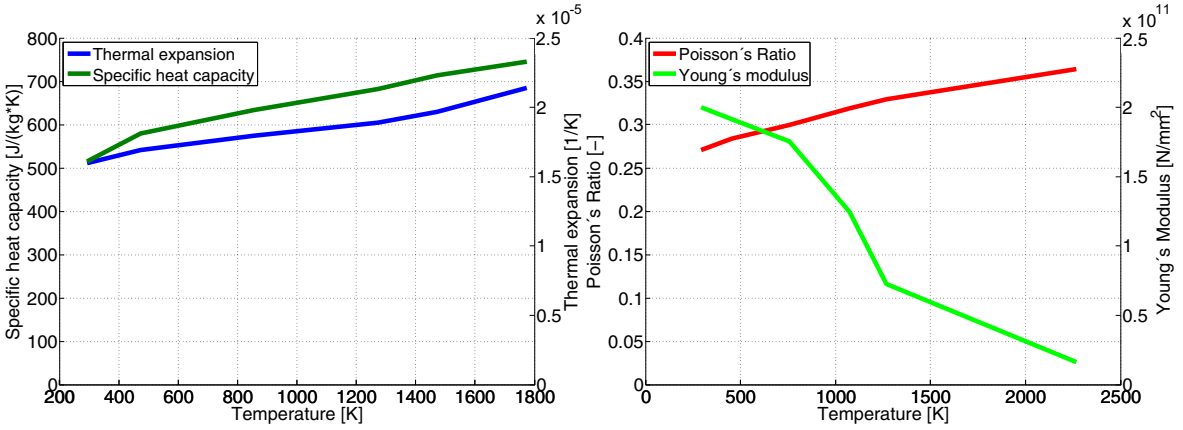

(a) Thermal properties

(b) Mechanical properties

Fig. 1: Material properties.

2.2. Heat sources

The experiments were carried out using a DC025 CO_2 laser from Rofin-Sinar Laser GmbH, with a wavelength of 10.6 µm, a handling system manufactured by SITEC Industrietechnologie GmbH and a spot diameter of 1 mm in focal position. The power was set to 2 kW and the travel speed of the sample carrier was adjusted to $2000\,\mathrm{mm\,min^{-1}}$. The second heat source is a diode laser from Laserline GmbH, LDM1000. The wavelength amounts to 980 nm. Due to the optical elements, a line spot geometry ($1\,\mathrm{mm} \times 16\,\mathrm{mm}$) can be obtained. The laser power was set to 300 W. The later position of the line spot was varied relative to the CO_2 spot. The angle of incidence was adjusted to 45° for the diode laser and 90° for the CO_2 laser. The side view of the experimental setup is shown in Fig. 2. In order to obtain information about the temperature distribution, thermocouples (type K) were placed next to the seam to measure the temperature on the upper surface of the sample.

2.3. Experimental setup

A straight-line welding trajectory of 280 mm was considered for the study. The samples were placed in a sample carrier and a clamping device fixed one plate. The other plate was free and the gap was set using two spacers made from the same material as the welding partners. The sample was released 75 s after the welding process started. In order to measure the displacement of the unclamped sheet, the current position was recorded with inductive probes (P2004, LVDT) manufactured by Mahr GmbH. The data was recorded with a universal recorder produced by Dewetron GmbH. The experimental setup is illustrated in Fig. 3.

2.4. Numerical modeling of the welding process

The numerical simulation was performed in the software Simufact.welding (Simufact Engineering GmbH). The thermal and mechanical temperature-dependent material properties used in the model are shown in Fig. 1 and are given from the software.

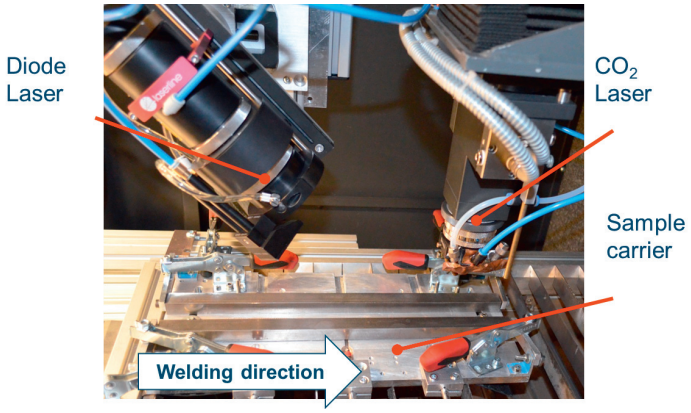

Fig. 2: Experimental setup (side view).

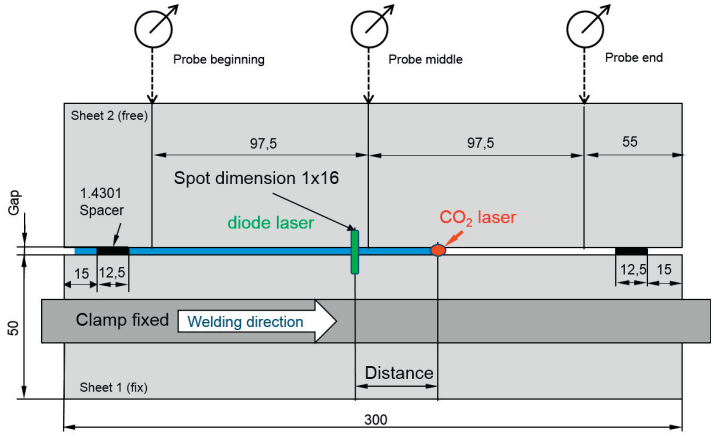

Fig. 3: Schematic illustration of the experimental setup (all sizes are in [mm]).

There are two different types of heat input present in the experiment: the CO_2 laser and the diode laser. The heat source for the first device is described in the numerical model as a volume and surface distributed laser source, which is composed of two parts: a Gauss surface distribution of the heat input and a constant heat distribution cylinder. The keyhole is modeled in the software using the following parameters: the radius of the molten cylinder, the radius of the surface source and the heat fraction. An illustration of the described parameters can be seen in Fig. 4(a).

For the general Gaussian distribution, the surface flux Q_r [W mm^{-2}] is expressed by Eq. 1, according to Goldak and Akhlagi (2005):

$$Q_r = Q_0 e^{-Cr^2} \tag{1}$$

where Q_0 [W mm^{-2}] is the maximum flux, r [mm] is the radial distance from the center of the heat source and C [mm^{-2}] is the distribution width coefficient.

For the particular case of laser beam welding, the heat flux is expressed as shown in Eq. 2:

$$Q_r = \frac{2\eta_e P_l}{\pi r_f^2} e^{\frac{-2r^2}{r_f^2}} \tag{2}$$

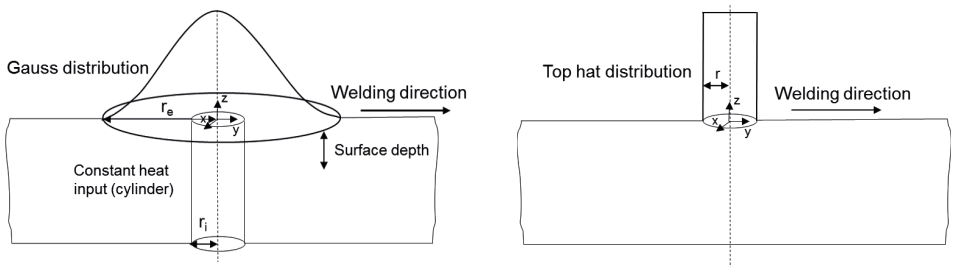

(a) Gaussian heat distribution (CO_2)

(b) Top hat heat distribution (diode laser)

Fig. 4: Heat source models.

where η_e is the process efficiency (the value being used is 0.59) and P_l is the power in W and r_f is the focus radius, as described in Goldak and Akhlagi (2005). For the diode laser, a top hat moving heat source distribution is used. The diode laser acts only on the upper surface of the plates and its representation is characterized by a constant surface distribution as seen in Fig. 4(b).

The pre-processing of the simulation model has been performed based on the experimental geometry and characteristics. For the 3D mesh, 8 node hexahedral elements, also known as brick elements, were used. The advantage of using this type of element is the increase in accuracy of the discretization in comparison with the more common tetrahedral elements, as well as a reduction of the computational time when compared with the high order elements according to ALGOR Development Staff (2011).

Fig. 5 shows the mesh of the computational model. The plates are placed on two supports and one of them is clamped. These elements act as boundary conditions. The welding simulation software allows the adaptive meshing based on the temperature gradients detected. This means that the mesh does not have to be very fine before the welding process commences, but as it progresses, it will be refined in the areas with higher temperature gradients by a coefficient of 0.1. The whole domain consists of 6006 elements and 8739 nodes.

Another aspect that is significant for the simulation result is the correct calibration of the heat transfer between the two welded plates. This is particularly important because, as mentioned earlier, the steel used has a low thermal conductivity, which means that the values for the convection, conduction and radiation have to be carefully calculated in order to ensure a realistic heat distribution, as seen in Perret et al. (2011).

The calibration of the numerical temperature field is defined by criteria such as the peak temperature, the width of the peak and the temperature distribution during the cooling time, as underlined in Balasubramanian et al. (2008). To establish the emissivity coefficient, thermographic camera measurements were carried out with both regular plates and plates painted black.

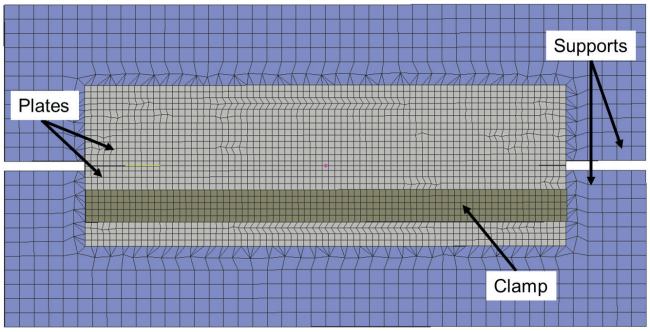

Fig. 5: Mesh.

2.5. Mathematical description of the heat transfer

A welding simulation is generally performed as a sequential simulation of the transient temperature field and the structural mechanics. The results can be divided then into two main categories: thermal and mechanica. In the case of laser beam welding, heat transfer can be calculated with the help of heat conduction theory. This leads to a coupling of the thermal and mechanical aspects of the problem, without taking a toll on the accuracy of the calculation, as described in Perret et al. (2011). The governing equation for the temperature field on the workpiece can be expressed as seen in Eq. 3, taking into account the moving coordinate system xyz which has the y axis along the welding trajectory, the z axis across the plate thickness and the origin at the surface of the plates, according to Balasubramanian et al. (2008):

$$\rho C_p \left[\frac{\partial T}{\partial t} + (-v_w) \frac{\partial T}{\partial y} \right] = \frac{\partial}{\partial x} \left(k \frac{\partial T}{\partial x} \right) + \frac{\partial}{\partial y} \left(k \frac{\partial T}{\partial y} \right) + \frac{\partial}{\partial z} \left(k \frac{\partial T}{\partial z} \right) + q_v(x, y, z) \tag{3}$$

The natural boundary condition associated with the heat transfer will then be as seen in Eq. 4.

$$k_n \frac{\partial t}{\partial n} - q + h(T - T_0) + \sigma \epsilon (T^4 - T_0^4) = 0 \tag{4}$$

Convective and radiative heat losses are also considered in the study. The initial condition for a transient analysis is displayed in Eq. 5 :

$$T(x, y, z, 0) = T_0(x, y, z) \tag{5}$$

It is important to notice that this thermo-mechanical simulation is coupled. The deformation of the plates is a consequence of the heat applied by the laser source, which determines the existence of stresses. This is why the thermal distribution is crucial for obtaining an accurate mechanical response in the simulation, according to Balasubramanian et al. (2008). The total time-dependent strain of a volume element in the material model is:

$$\epsilon = \epsilon_i + \epsilon_e + \epsilon_p + \epsilon_{th} \tag{6}$$

where ϵ_i is the initial strain, ϵ_e is the elastic strain, ϵ_p is the plastic strain and ϵ_{th} is the thermal strain. The initial strain is taken as 0 at this point of the project, as residual stress from previous machining is not taken into consideration in the model. The elastic strain for an isotropic material is given by equation Eq. 7:

$$\epsilon_e = [D]^{-1} \cdot \sigma \tag{7}$$

where [D] is the stress-strain matrix and σ is the stress. The plastic strain can be obtained from Eq. 8:

$$d\epsilon_p = d\lambda \cdot \frac{\partial f^{vM}}{\partial \sigma} \tag{8}$$

where f^{vM} is the plastic potential, $d\lambda$ is the hardening parameter and σ is the stress. The thermal strain is calculated from Eq. 9.

$$\epsilon_{th} = \alpha(T) \cdot (T - T_0) \tag{9}$$

where $\alpha(T)$ is the temperature dependent thermal expansion coefficient, T_0 is the reference temperature and T is the temperature, as stated in Hildebrand (2008). The model used for the material hardening is an isotropic one, therefore the yield surface extends with accumulate plastic strain. The yielding occurs when:

$$f = \sigma_{eq} - K - \sigma_y = 0 \tag{10}$$

where σ_{eq} is the von Mises equivalent stress, σ_y is the initial yield stress and K is the degree of strain hardening, referenced from Mullins and Gunnars (2009). The software uses the sfMarc solver with the option Parallel Direct Sparse Solver to perform the FE interpolation for the thermo-mechanical analysis. The simulations were run in parallel on 8 processors. The time step is automatically calculated based on the element size by using the formula:

$$\Delta t = \frac{l}{2^{n_1} v_w n_2} \tag{11}$$

A generally accepted method for numerical model validation is comparing the numerical results with the ones coming from the experiment. The fact is that numerical models can represent physical effects only to a certain extent. Keeping this is mind, it is important to identify some causes for the uncertainties existent in the model, such as unknown effective material parameters and their statistical properties, as can be read in Sudnik et al. (2000).

The numerical model proposed has been validated by comparison of the temperature curves plotted in time with the ones measured in the experiment at predetermined measuring points. This is visible in Fig. 6. The plot shows a good agreement between the experiment and simulation temperature curves.

3. Results and conclusions

The experiments and numerical simulation results have shown a high in-plane and out-of-plane displacement of the steel sheets caused by the laser welding process. The unclamped sheet deforms freely causing an increase of the gap at the two ends of the trajectory, affecting the welding process in a negative way. Consequently, the laser is focused just on the clamped sheet, the other one being outside of the laser spot area. This can be seen in Fig. 7, taken from the numerical simulation. The yellow region denotes the molten zone whereas the dark red symbolizes the heat-affected zone.

In Fig. 8, the time dependent course of the displacement is illustrated. With the start of the welding process, the displacement commences and keeps increasing. After the welding process a gradual negative displacement can be observed, which is an effect of the cooling. Fig. 9 shows the displacement with the second heat source active. When the diode laser is activated, a slight fluctuation in the displacement can be identified. The maximum displacement at all the points is lower using the second heat source. Due to the level mechanism, the center of rotation is the weld bead, the values of the probes at the end position being higher than in the middle and start point.

Even though the two lasers are active until a predetermined end-point, it is observed that because of the disruption seen in Fig. 7, the effective welding of the two plates stops before this point. The interval in which a good weld bead

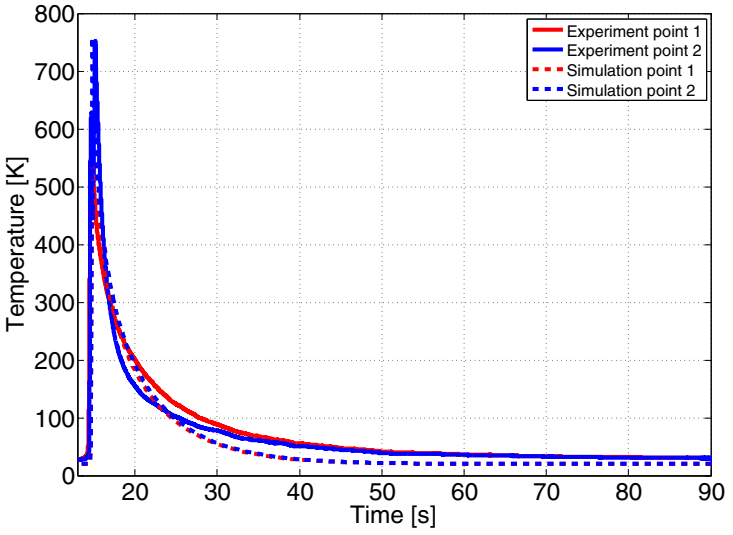

Fig. 6: Numerical validation for the CO_2 heat source.

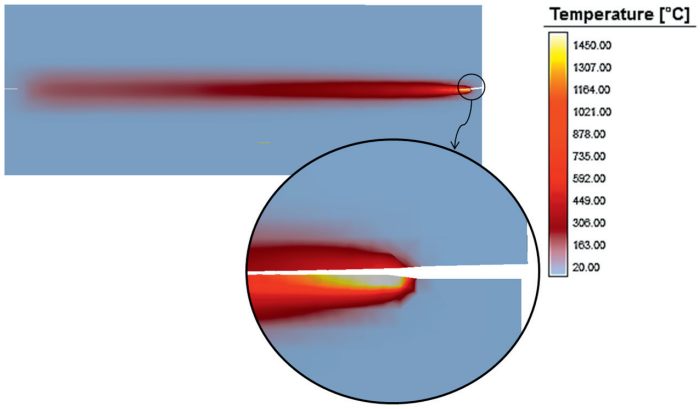

Fig. 7: Defect caused by large displacements at the ends of the weld trajectory (scaled by a factor of 3).

is obtained is marked in Fig. 8 and Fig. 9. The out of plane displacement is caused by the compressive stresses present in the middle part of the upper surface of the sheets. The outcome is an increase in concavity of the unclamped plate.

The influence of the distance between the CO_2 laser and the diode laser for a gap width of 0.05 mm and 0.1 mm is illustrated in Fig. 10 and Fig. 11. For the particular cases taken into consideration, less displacement is observed for a gap width of 0.1 mm and a distance between the two heat sources of 50 mm. The trend of the maximum displacement obtained in the simulation is in agreement with the experimental data. One conclusion that can be drawn from these results is the possibility to control and diminish the deformations generated by the laser welding process by varying the distance between the two sources.

The influence of the working speed of the CO_2 laser on the welding process has been previously studied. At higher working speeds, the displacement and stresses have lower values. This can be explained in terms of how much heat is

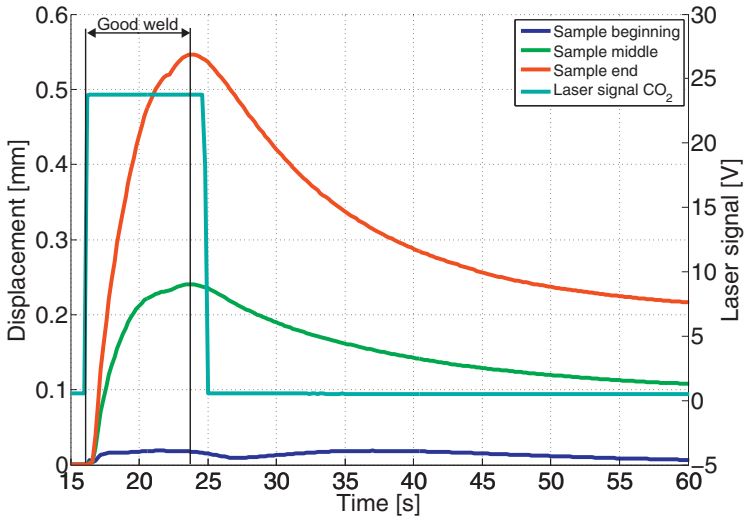

Fig. 8: Time dependent course of the displacement in the experiment without the diode laser for P=2 kW, v=2000 mm min^{-1}, measured at the points seen in Fig. 3.

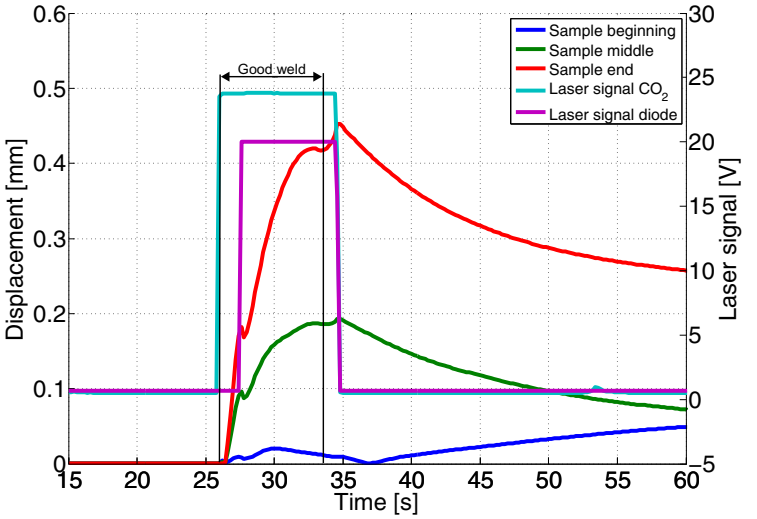

Fig. 9: Time dependent course of the displacement in the experiment (distance between diode laser and CO_2 laser is 50 mm, the gap distance is 0.05 mm), P_{CO_2}=2 kW, v=2000 mm min^{-1}, P_{Diode}=0.3 kW, measured at the points seen in Fig. 3.

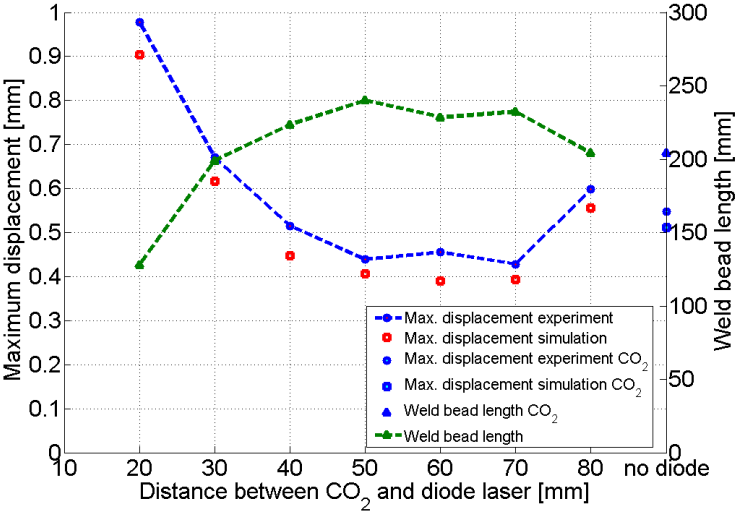

Fig. 10: Influence of the position of the second heat source on the weld length and maximum deflection for a gap of 0.05 mm.

absorbed by the material, therefore by the dimension of the weld pool and the HAZ. An equally important parameter is the power input. After concluding that its effect is inversely proportional to that of the working speed, the CO_2 laser power was kept constant at P = 2 kW in order to accurately observe the influence of the second heat source.

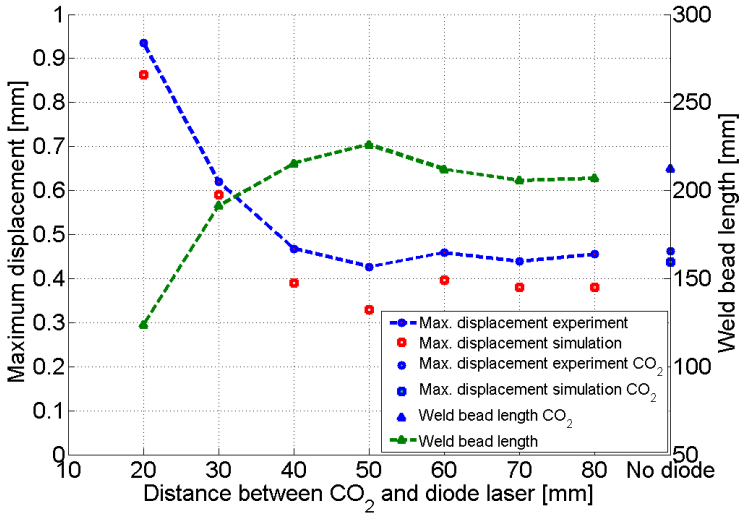

Fig. 11: Influence of the position of the second heat source on the weld length and maximum deflection for a gap of 0.1 mm.

Acknowledgment

The investigations were carried out within the project ”Optimization strategies for welding high alloyed steel sheets” (01.04.2013 - 31.03.2015). The research project (IGF-00.476 ZBR) is supported by the Federal Ministry of Economic Affairs and Energy within the Allianz Industrielle Forschung (AIF), which is based on a resolution of the German Parliament. We would like to thank all funding organizations.

References

Edelstahl Rostfrei, Schweissen Merkblatt 823, Oct.2007.

Zhao, H., Wang, X., Wang, X.C., Lei, Y., 2008. Reduction of residual stress and deformation in electron beam welding by using multiple beam technique. Front. Mater. Sci. China 2(1), 66-71.

Simon, F., Nagel, F., Hildebrand, J., Bergmann, J.P., 2013. “Optimization strategies for welding high-alloy steel sheets”. Förderverein der numerischen Analyse der Wärmebehandlungs- und Schweissprozesse Simulationsforum 2013, Weimar, Germany, paper #19.

Petzet, V., Büskens, C., Pesch, H.J., Karkhin, V., Makhutin, M., Prikhodovsky, A., Ploshikhin, V., 2005. Numerical Optimization as a Key Tool for the Improvement of Advanced Multi-Beam Laser Welding Techniques, High Performance Computing in Science and Engineering. Springer, Garching, pp. 153-166.

Goldak,J., Akhlagi,M., 2005. Computational Welding Mechanics.Springer, Ottawa, pp.26-27.

ALGOR Development Staff, The eight-node hexahedral ”brick” element in finite element analysis, May 2011.

Perret,W., Thater R., Alber U., Schwenk C. Rethmeyer M., 2011. Approach to assess a fast welding simulation in an industrial environment - application for an automotive welded part. International Journal of Automotive Technology 6, 895-901.

Balasubramanian, K.R., Shanmugam, S., Buvanashekaran, G., Sankaranarayanasamy, K., 2008. Numerical and experimental investigation of laser beam welding of AISI 304 stainless steel sheet.Advances in Production Engineering & Management 3, 93-105.

Hildebrand, J.,2008. Numerische Schweisssimulation: Bestimmung von Temperatur, Gefüge und Eigenspannung an Schweissverbindungen aus Stahl- und Glaswerkstoffen. Bauhaus-Universität Weimar, Weimar, pp.59-61.

Mullins, J., Gunnars, J., Influence of Hardening Model on Weld Residual Stress Distribution. Report for 2009, Swedish Radiation Safety Authority, Jan. 2009.

Sudnik, W., Radaj, D., Breitschwerdt, S., Erofeew, W., 2000. Numerical Simulation of weld pool geometry in laser beam welding. Journal of Physics D 33, 662-671.